Filipe Marques
Departamento de Engenharia Mecânica
Universidade do Minho, Campus de Azurém
4804-533 Guimarães, Portugal
E-mail: fmarques@dem.uminho.pt

Nuno Dourado
Departamento de Engenharia Mecânica
Universidade do Minho, Campus de Azurém
4804-533 Guimarães, Portugal
E-mail: nunodourado@dem.uminho.pt

Paulo Flores
Departamento de Engenharia Mecânica
Universidade do Minho, Campus de Azurém
4804-533 Guimarães, Portugal
E-mail: pflores@dem.uminho.pt

Fernando Isaac
Departamento de Engenharia Mecânica
Universidade do Minho, Campus de Azurém
4804-533 Guimarães, Portugal
E-mail: efinhoisaac@hotmail.com

António Pedro Souto
2C2T/Departamento de Engenharia Têxtil
Universidade do Minho, Campus de Azurém
4804-533 Guimarães Portugal
E-mail: souto@det.uminho.pt

Hamid M. Lankarani
Department of Mechanical Engineering,
Wichita State University
Wichita, KS 67260-133
E-mail: hamid.lankarani@wichita.edu

ABSTRACT

An investigation on the dynamic modeling and analysis of spatial mechanisms with spherical clearance joints including friction is presented. For this purpose, the ball and the socket which compose a spherical joint are modeled as two individual colliding components. The normal contact-impact forces that develop at the spherical clearance joint are determined by using a continuous force model. A continuous analysis approach is used here with a Hertzian based contact force model, which includes a dissipative term representing the energy dissipation during the contact process. The pseudo-penetration that occurs between the potential contact points of the ball and the socket surface, as well as the indentation rate play a crucial role in the evaluation of the normal contact forces. In addition, several different friction force models based on the Coulomb's law are revisited in this work. The friction models utilized here can accommodate the various friction regimens and phenomena that take place at the contact interface between the ball and the socket. Both the normal and tangential contact forces are evaluated and included into the systems' dynamics equation of motion, developed under the framework of multibody systems formulations. A spatial four bar mechanism, which includes a spherical joint with clearance, is used as an application example to examine and quantify the effects of various friction force models, clearance sizes, and the friction coefficients.

1. INTRODUCTION

The problem of modeling and simulating joints with clearances in mechanisms is a research area with much interest in different fields, and has attracted the attention of many authors over the last two decades. This interest has led to the development of relevant work and publication of a number of studies on dry and lubricated revolute joints [1-10], translational joints with clearance [11-16], cylindrical joints with clearance [17-19], and experimental investigations [20-24]. Most of these studies are devoted to planar mechanisms, such as the four bar linkage, slider-crank mechanism, and robot manipulators, in which one, two or more joints have clearance features. On the subject of modeling three-dimensional systems with clearance joints, research works mostly deal with spherical joints with clearance, where the surface compliance properties, and clearance size are taken into account. Some typical and important mechanical systems in which spherical joints with clearance play a key role are the vehicle systems and components, such as steering, suspensions, and bushing joints [25, 26], robotic and parallel manipulators [27], space deployable systems [28], and natural and artificial human articulations, namely for the hip and shoulder cases [29-31].

Indeed, a number of works devoted to the spherical joints with clearance has been carried out over the last few years.

Some of them focus on systems in which only one joint is modeled as a realistic joint. Bauchau and Rodriguez [32], based on the finite element dynamic analysis of nonlinear flexible multibody systems, proposed a formulation for mechanisms with revolute and spherical joints with clearance. The effects of structural damping and driving speed were investigated. Orden [33] presented a methodology for the study of typical smooth joint clearances in multibody systems. The proposed approach takes advantage of an analytical definition of the material surfaces defining the clearance, resulting in a formulation where the gap does not play a central role, as it happens in standard contact models. This approach has been demonstrated as an effective and efficient method in solving the equations of motion. Liu et al. [34] developed a contact force formulation of the spherical clearance joints in multibody mechanical systems, using the distributed elastic forces to model the compliance of the surfaces in contact. Flores et al. [35] presented an analytical methodology to assess the influence of the spherical joint clearances in spatial multibody mechanical systems. This approach is only valid for the case of dry frictionless contact between the socket and ball. Tian and his co-authors [36] presented a computational formulation for dynamic analysis of three-dimensional flexible multibody systems, considering the effects of the clearances and lubrication for the case spherical joints. The friction effect at the contact was simply accounted using the Coulomb's friction law. The effectiveness of the methodology proposed was demonstrated by different numerical examples.

More recently, Wang et al. [37] investigated on the wear phenomena in spherical joints with clearance. For this purpose, the well-known Archard's wear model was considered and incorporated into the dynamics equations of motion for constrained multibody mechanical systems. This approach was validated using the finite element method. Wang and Liu [38] studied the response of a 4-SPS/CU parallel mechanism which includes a spherical joint clearance. In this investigation, an enhanced contact force models has been proposed to deal with the normal contact-impact analysis between the joint elements. Besides its limitations, the Coulomb's law was considered to account for the friction action at the joint clearance. Jing et al. [28] analyzed the nonlinear behavior of spherical joints with clearance considering the classical Winkler contact approach to propose a new formulation to define the contact stiffness when the radial clearance is small, and therefore the Hertzian contact theory cannot be applied. The proposed formulation was validated against the response from a finite element model. Zheng et al. [39] investigated the dynamics of rigid-flexible spatial multibody systems with spherical joints with clearance, with particular emphasis on the response of ultra-precision presses.

The present investigation extends previous authors' work [35] to incorporate the frictional effects when modeling spherical joints with clearance. In this process, several different friction force models based on the dry Coulomb's friction law are discussed and utilized. In a simple manner, the components that constitute a spherical joint with clearance are modeled as colliding bodies. The dynamic response of the joint, in terms of contact-impact and friction forces, is influenced by the geometric and material properties of the contacting surfaces, as well as by the joint kinematics. The intra-joint contact forces are determined during the contact period in a continuous manner, and then incorporated into the equations of motion as external applied forces. The remaining of this paper is organized as follows. Section 2 deals with the main kinematic aspects of spherical clearance joints. The numerical models for the normal contact and tangential friction forces are described in Section 3. The dynamics equations of motion for constrained spatial multibody mechanical systems are also presented in this section. Numerical results obtained from computational simulations of a spatial four bar mechanism with frictional spherical clearance are analyzed in Section 4. Finally, the main conclusions of this investigation are drawn in Section 5.

2. MODELING SPHERICAL CLEARANCE JOINTS

A mathematical model for the spherical joint with clearance, under the framework of multibody systems formulation, is briefly described in this section, which closely follows the work by Flores et al. [35]. Figure 1 illustrates two links i and j of a typical connection with a generic spherical joint with clearance in mechanisms. As Fig. 1 illustrates, the radii of socket and ball are R_i and Rj, respectively. The difference in radius between the socket and the ball provides the radial clearance, $c = R_i - R_j$.
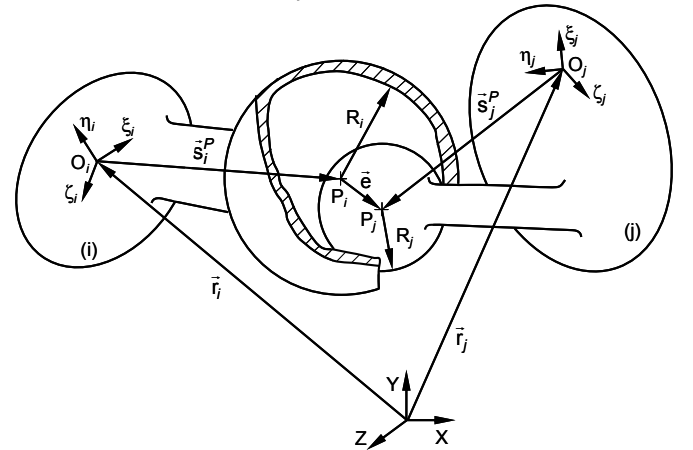

Figure 1: General representation of a typical spherical joint with clearance in spatial mechanisms

Referring to Fig. 1, the relative penetration or deformation vector between the ball and socket walls can be defined as

$$\boldsymbol{\delta} = \mathbf{e} - (R_i - R_j)\mathbf{n} \qquad (1)$$

where $\mathbf{e}$ is the eccentricity vector, and $\mathbf{n}$ represents the normal vector which defines the normal direction of the plane of collision. The eccentricity vector $\mathbf{e}$ is given by

$$\mathbf{e} = \mathbf{r}_j^P - \mathbf{r}_i^P \qquad (2)$$

where both $\mathbf{r}_j^P$ and $\mathbf{r}_i^P$ are defined as [40]

$$\mathbf{r}_k^P = \mathbf{r}_k + \mathbf{A}_k \mathbf{s}_k'^P \qquad (k = i, j) \qquad (3)$$

Fig. 2 depicts the case where the socket and the ball surfaces are in contact, which is identified by the existence of a relative indentation or pseudo-penetration, δ. The contact points on bodies i and j are Q_i and Q_j, respectively. The position of the contact points in the socket and ball can be evaluated as

$$\mathbf{r}_k^Q = \mathbf{r}_k + \mathbf{A}_k \mathbf{s}_k'^P + R_k \mathbf{n} \qquad (k = i, j) \qquad (4)$$

The velocities of the contact points Q_i and Q_j in the global system are obtained by differentiating Eq. (4) with respect to time, yielding

$$\dot{\mathbf{r}}_k^Q = \dot{\mathbf{r}}_k + \dot{\mathbf{A}}_k \mathbf{s}_k'^P + R_k \dot{\mathbf{n}} \qquad (k = i, j) \qquad (5)$$

The relative scalar velocities, normal and tangential to the plane of collision are found by projecting the relative impact velocity onto each one of these directions as follows

$$\mathbf{v}_N = [(\dot{\mathbf{r}}_j^Q - \dot{\mathbf{r}}_i^Q)^T \mathbf{n}]\mathbf{n} \qquad (6)$$

$$\mathbf{v}_T = (\dot{\mathbf{r}}_j^Q - \dot{\mathbf{r}}_i^Q) - \mathbf{v}_N \equiv v_T \mathbf{t} \qquad (7)$$

where $\mathbf{t}$ represents the tangential direction to the impact surfaces.
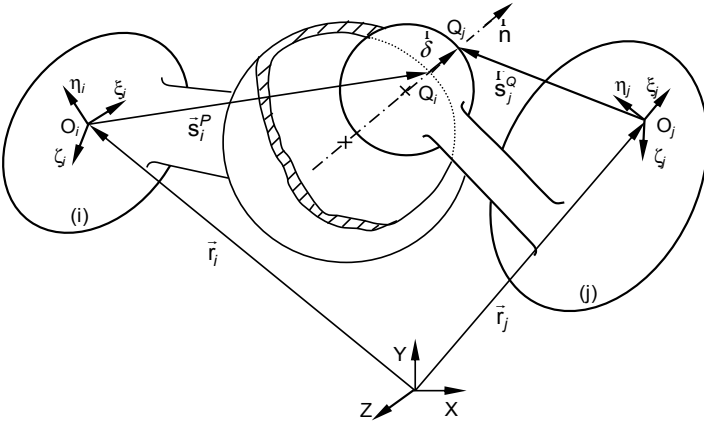

Figure 2: Relative indentation between the ball and socket

3. MODELS FOR CONTACT-IMPACT FORCES

In this section, numerical models for the evaluation of the normal and tangential contact-impact and friction forces, which develop at the spherical clearance joints, are presented. The normal and tangential forces at the contact points are represented by $\mathbf{f}_N$ and $\mathbf{f}_T$, respectively. Since these forces do not act through the center of mass of bodies i and j, the moment components for each body need to be evaluated.

The elastic force developed in the contact between the ball and socket can be modeled using a Hertzian-type contact law, which can be expressed as [41]

$$F_N = K \delta^n \qquad (8)$$

where F_N denotes the contact force, K represents a generalized stiffness parameter and δ is the relative penetration depth. The generalized contact stiffness depends on the material properties and on the geometry of the contacting bodies. For two spheres in contact, the stiffness coefficient is a function of the radii of the spheres i and j and the material properties as [42]

$$K = \frac{4}{3(\sigma_i + \sigma_j)} \sqrt{\frac{R_i R_j}{R_i + R_j}} \qquad (9)$$

where R_i and R_j are the radii of the spheres and σ_i and σ_j are given by

$$\sigma_k = \frac{1 - v_k^2}{E_k} \qquad (k = i, j) \qquad (10)$$

and the quantities v_k and E_k are the Poisson's ratio and the Young's modulus associated with each sphere, respectively.

The Hertz contact law is a purely elastic model, and it does not include any energy dissipation. Lankarani and Nikravesh [43] extended the Hertz contact law to include the energy dissipation in terms of internal damping as

$$F_N = K \delta^n \left[1 + \frac{3(1 - c_r^2)}{4} \frac{\dot{\delta}}{\dot{\delta}^{(-)}} \right] \qquad (11)$$

where the generalized parameter K is evaluated by Equations (9) and (10) for sphere to sphere contact, or by similar expressions for the contact of other types of geometries, c_r is the restitution coefficient, $\dot{\delta}$ is the instantaneous relative normal penetration velocity and $\dot{\delta}^{(-)}$ is the initial relative normal contact-impact velocity where contact is detected.

Alternative normal contact force models have been developed over the last years, which can accommodate different levels of energy dissipation and enhanced ways to deal with the contact stiffness for conformal and nonconformal contacts. Other contact models which include energy dissipation may be utilized instead. Hence, this issue is out of the scope of the present work, and the interested reader referred to the work by Alves et al. [44].

In what follows, some of the most significant friction force models are presented, which will be utilized later. Over the last decades, several researchers have investigated the modeling of frictional effects in mechanical systems [45-47]. The dry Coulomb friction model [48] is the most popular and well-known friction force model. This approach states that friction always oppose the relative motion between two contacting bodies, and its magnitude is proportional to the normal contact force, as illustrated in Fig. 3a. The Coulomb's friction force model can be expressed as follows

$$\mathbf{f}_T = \begin{cases} F_C \hat{\mathbf{v}}_T & \text{if } v_T \neq 0 \\ \min\left(\|\mathbf{F}_e\|, F_C \right) \hat{\mathbf{F}}_e & \text{if } v_T = 0 \end{cases} \qquad (12)$$

where

$$F_C = \mu_k \|\mathbf{f}_N\| \qquad (13)$$

in which F_C denotes the magnitude of Coulomb friction, $\mathbf{F}_e$ is the external tangential force, μ_k represents the kinetic coefficient of friction, and $\hat{\mathbf{v}}_T$ denotes a unit vector with the same direction of $\mathbf{v}_T$. This friction force model is mathematically simple; however, it introduces several numerical difficulties to implement due to the existing discontinuity at zero velocity.

Several modifications of Coulomb's law have been proposed to eliminate the discontinuity and, therefore, enhance the computational efficiency during dynamic simulations [49-51]. Ambrósio [51] suggested a modified Coulomb's friction law with a tolerance around zero velocity, which is represented in Fig. 3b, and can be given as

3

$$\mathbf{f}_T = \begin{cases} \mathbf{0} & \text{if } v_T \leq v_0 \\ \dfrac{v_T - v_0}{v_1 - v_0} F_C \hat{\mathbf{v}}_T & \text{if } v_0 < v_T < v_1 \\ F_C \hat{\mathbf{v}}_T & \text{if } v_T \geq v_1 \end{cases} \tag{14}$$

where v_0 and v_1 are tolerance velocities.

Threlfall [49] proposed a friction force model in which the force and velocity are related by an exponential function with the purpose of addressing the numerical difficulties associated with the discontinuity in the Coulomb's law. This was the basis for other friction force models, namely the continuous function, depicted in Fig. 3c, and expressed as

$$\mathbf{f}_T = F_C \tanh\left(\frac{v_T}{v_1}\right) \hat{\mathbf{v}}_T \tag{15}$$

It is well known from experiments that the coefficient of friction is not a constant value. Thus, two different coefficients of friction must be considered, namely "static" and "kinetic" coefficients. Stribeck [52] showed experimentally that, for low velocities, friction decreases with the increase of the relative velocity, as plotted in Fig. 3d. This curve can be written as [53]

$$\mathbf{f}_T = \left(F_C + (F_S - F_C) e^{-\left(\frac{v_T}{v_S}\right)^2} \right) \hat{\mathbf{v}}_T \tag{16}$$

where

$$F_S = \mu_s \|\mathbf{f}_N\| \tag{17}$$

in which F_S represents the magnitude of static friction force, μ_s denotes the static coefficient of friction, and v_S is the Stribeck velocity. Similarly to Coulomb's law, this approach contains a discontinuity for the null velocity. In order to avoid numerical difficulties, a model with tolerance at zero velocity and linear interpolation can be considered, as represented in the plot of Fig. 3e. In this way, friction force can be described as

$$\mathbf{f}_T = \begin{cases} \left(\dfrac{v_T}{v_0} F_S\right) \hat{\mathbf{v}}_T & \text{if } v_T \leq v_0 \\ \left(F_S - \dfrac{v_T - v_0}{v_1 - v_0} (F_S - F_C) \right) \hat{\mathbf{v}}_T & \text{if } v_0 < v_T < v_1 \\ F_C \hat{\mathbf{v}}_T & \text{if } v_T \geq v_1 \end{cases} \tag{18}$$

Bengisu and Akay [54] presented an alternative approach to deal with the discontinuities associated with the Coulomb's friction law. Recurring to a few modifications, this model is represented in Fig. 3f, and expressed as

$$\mathbf{f}_T = \begin{cases} \left(-\dfrac{F_S}{v_0^2} (v_T - v_0)^2 + F_S \right) \text{sgn}(\mathbf{v}_T) & \text{if } v_T < v_0 \\ \left(F_C + (F_S - F_C) e^{-\xi(v_T - v_0)} \right) \text{sgn}(\mathbf{v}_T) & \text{if } v_T \geq v_0 \end{cases} \tag{19}$$

in which ξ should be a positive parameter representing the negative slope of the sliding state.

The normal contact forces and the frictional forces and their corresponding motion at the center of mass are hence evaluated as described in this section, and then included in the dynamics equations of motion. The dynamics equations of motion for a multibody system subjected to holonomic constraints can be state in the form [40]

$$\begin{bmatrix} \mathbf{M} & \mathbf{\Phi}_q^T \\ \mathbf{\Phi}_q & \mathbf{0} \end{bmatrix} \begin{Bmatrix} \ddot{\mathbf{q}} \\ \lambda \end{Bmatrix} = \begin{Bmatrix} \mathbf{g} \\ \gamma \end{Bmatrix} \tag{20}$$

with the reference frame placed at the center of mass for each body, $\mathbf{M}$ is the system mass matrix, $\mathbf{\Phi}_q$ is the Jacobian matrix of constraint equations, vector $\ddot{\mathbf{q}}$ contains the generalized state accelerations, λ is the vector that contains the Lagrange multipliers associated with the kinematic constraints, $\mathbf{g}$ is the vector of generalized forces, and γ is the vector of quadratic velocity terms in the kinematic acceleration equation. Moreover, the general state coordinates $\mathbf{q}$ must be defined within a Cartesian reference system, and consists of three translational coordinates (x, y and z) and four Euler parameters to specify the angular orientation (e_0, e_1, e_2 and e_3) [40].
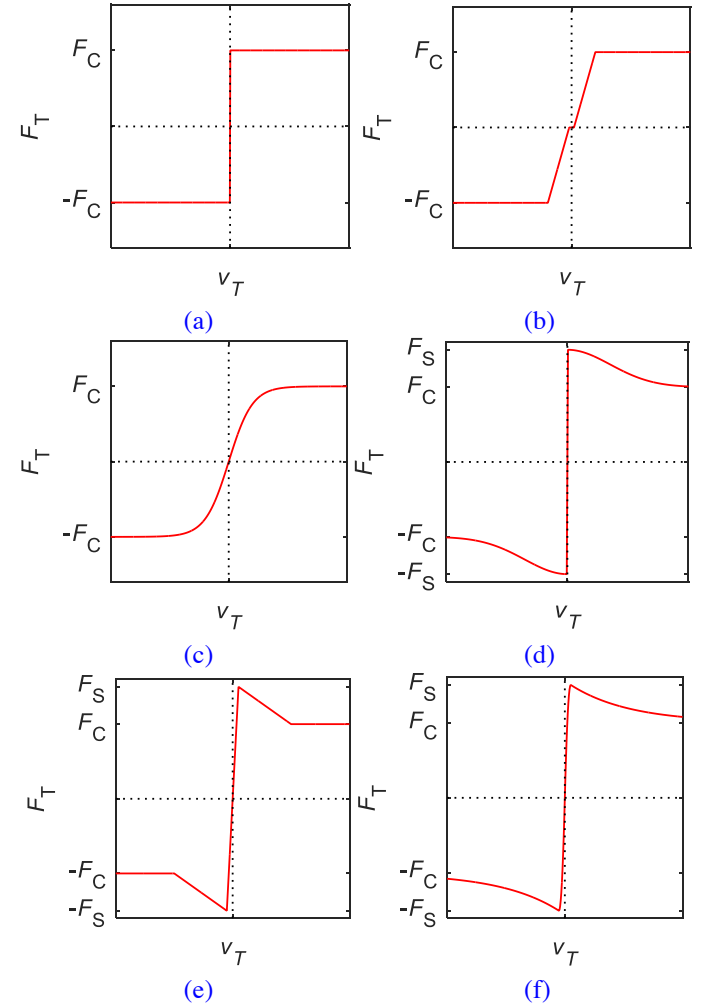

Figure 3: Behavior of the friction force models: (a) Coulomb, (b) Ambrósio, (c) Threlfall, (d) Stribeck, (e) Piecewise-linear, (f) Bengisu and Akay.

Equation (20) is formed as a combination of the equations of motion and kinematic constraint equations, often referred to

as a mixed set of differential and algebraic equations. A set of initial conditions is required to start the dynamic simulation. The selection of the appropriate initial conditions plays a key role in the prediction of the dynamic performance of mechanical system. In the present work, the initial conditions are derived from the kinematic simulation of the mechanical system with ideal joints; i.e., with no clearance [40]. In order to stabilize the constraints violation, Eq. (20) is solved using the Baumgarte stabilization method [55, 56]. This spatial multibody formulation is implemented on an in-house developed MATLAB code. In the present work, the integration process is performed using a predictor-corrector algorithm, namely with the *ode15s* solver which is included in MATLAB's library.

4. NUMERICAL RESULTS AND DISCUSION

In this section, the application of the spatial four bar mechanism is utilized as an illustrative example to show how modeling approaches for a spherical joint clearance with friction can affect the behavior of the mechanism [35]. This mechanism consists of four rigid links that represent the ground, crank, coupler and rocker. The body numbers and their corresponding local coordinate systems are shown in Fig. 4. The kinematic joints of this model include two ideal revolute joints, connecting the ground to the crank and the ground to the rocker, and an ideal spherical joint connecting the crank and the coupler. A spherical clearance joint connects the coupler and rocker. This system is modeled with twenty four Cartesian coordinates (including ground), which result from the four rigid links and nineteen kinematic constraints. Hence, this system has five degrees-of-freedom.
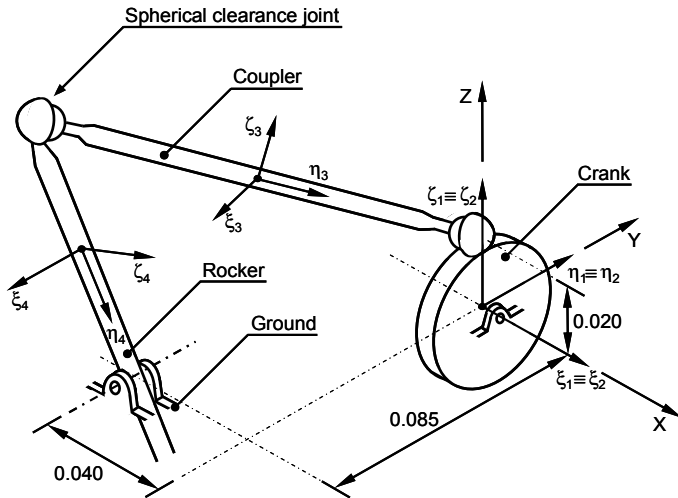

Figure 4: Schematic representation of the spatial four bar mechanism with a spherical clearance joint

The initial configuration of the spatial four bar mechanism is illustrated in Fig. 4, and the initial values are displayed in Table 1. The system is released from the initial position with null velocities and under the action of gravitational force, which is taken to act in the negative *z*-direction. Initially the ball and socket are concentric. The dimensions and inertia properties of each body are presented in Table 2.

Table 1: Initial configuration for the spatial four bar mechanism

Body Nr.	x [m]	y [m]	z [m]	e_0	e_1	e_2	e_3
2	0.00000	0.00000	0.00000	1.0000	0.0000	0.0000	0.0000
3	-0.03746	-0.04250	0.04262	0.9186	-0.1764	0.6747	-0.3472
4	-0.05746	-0.08500	0.03262	0.3634	-0.6068	-0.6068	0.3634

Table 2: Properties of the spatial four bar mechanism

Body Nr.	Length [m]	Mass [kg]	Moment of inertia [kgm^2]		
			$I_{\xi\xi}$	$I_{\eta\eta}$	$I_{\zeta\zeta}$
2	0.020	0.0196	0.0000392	0.0000197	0.0000197
3	0.122	0.1416	0.0017743	0.0000351	0.0017743
4	0.074	0.0316	0.0001456	0.0000029	0.0001456

The parameters utilized for the dynamic simulations and for the numerical methods required to solve for the system's dynamic response, are listed in Table 3.

In what follows, several numerical results obtained from various computational simulations are considered to show the response of the spatial four bar mechanism for three distinct situations, namely: ideal spherical joint, frictionless spherical joint with clearance, and spherical joint with clearance and friction. The parameters and coefficient utilized for the friction force models considered are listed in Table 4.

Table 3: Simulation parameters for the four bar mechanism

Joint socket radius	10.0 mm
Joint ball radius	9.8 mm
Restitution coefficient	0.9
Young's modulus	207 GPa
Poisson's ratio	0.3
Baumgarte coefficient - α	5
Baumgarte coefficient - β	5
Integrator algorithm	ode15s
Reporting time step	0.00001s
Integration tolerance	10^{-10}
Simulation time	2 s

Table 4: Simulation parameters for the friction models

Kinetic coefficient of friction - μ_k	0.1
Static coefficient of friction - μ_S	0.15
Velocity tolerance - v_0	0.0001 m/s
Velocity tolerance - v_1	0.001 m/s
Factor for curve shape - ξ	1000 s/m

Figures 5a-c show the *z*-component of the position, velocity and acceleration of the rocker center of mass, respectively. From these plots, it can be observed that the modeling of the spherical joint can significantly affect the dynamic performance of the system. Overall, the frictionless joint model exhibits more oscillations, in particular for the velocity and acceleration plots. This suggests that the system's response becomes chaotic in this case due to the higher peaks visible at the acceleration level. Figures 5a-c also indicate that the spatial four bar mechanism with the spherical joint clearance produces significantly larger velocities and accelerations, when compared with the ideal joint case. In turn,

the simulation with the spherical clearance joint using the Threlfall based friction model shows a smoother behavior. This effect is quite visible in the plots represented in Figs. 5a-c. Moreover, the mechanical energy dissipated is higher for the case with friction, as it observed in the plots of Fig. 5d. This effect is evident in the measure that the energy loss is only due to the forces generated at the spherical clearance joint.

Figure 6 shows the relative position of the ball and socket centers for both frictionless clearance joint and clearance joint with friction. In these two cases, the main impacts occur in the initial phase. The frictionless joint exhibits higher number of impacts that are followed by rebounds when compared with the case with friction. In fact, the dissipative and damping effect associated with friction phenomenon promotes the continuous contact between the ball and socket surfaces.

The phase portraits are commonly utilized to study the level the nonlinearity associated with the system's response. In the present work, the z-component of position versus velocity, and velocity versus acceleration, are the variables considered to plot the phase space portraits, as displayed in Fig. 7. From the analysis of these plots, it can be observed that the four bar mechanism has a quite nonlinear behavior when the spherical joint clearance is modeled as frictionless contact. This phenomenon is clearly associated with the level and degree of the impacts between the ball and socket surfaces. In fact, when there is no friction, the system needs more time to ensure a continuous or permanent contact between the joint elements. Moreover, it is evident that initial impacts are followed by rebounds. This effect is visible in plots of Figs. 7c-d and Fig. 6a, in which the system changes form free-flight mode to impact mode. This particular phenomenon has consequences in the phase portraits, which are of more complex nature, as depicted in Fig. 7d. In contrast, when the system is modeled with the Threlfall based friction model, the dynamic behavior tends to be smoother and closer to the ideal or perfect joint case, as observed in the diagrams of Fig. 7e-f. This behavior can be understood from the dissipative nature related to the friction effect, which facilitates the accommodation between the ball and socket surfaces. When the system is modeled with friction, it produces less and smaller impacts, as observed again in the smooth nature of Figs. 7e-f.
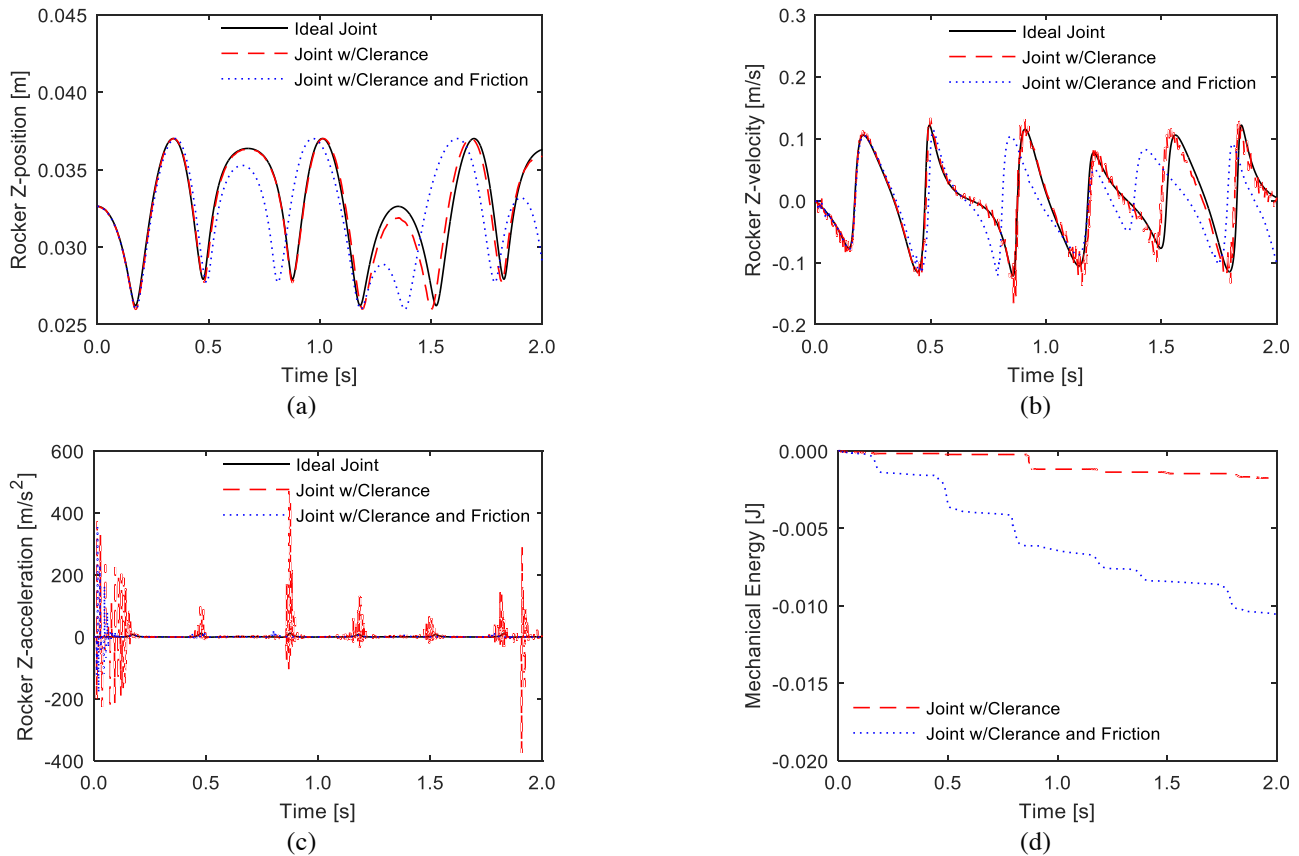

Figure 5: (a) Z-position of the rocker, (b) Z-velocity of the rocker, (c) Z-acceleration of the rocker; (d) Mechanical energy variation

6
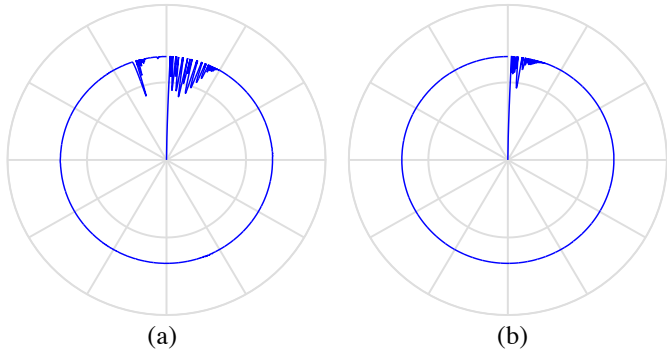
Figure 6: Eccentricity ratio evolution with time: (a) frictionless clearance joint; (b) clearance joint with friction

It has been shown that friction has a significant effect on the dynamic response of the four bar mechanism with a spherical clearance joint. With the purpose of examining the influence of the friction force model utilized in the dynamic simulations of the mechanisms, four different approaches are considered here, namely Ambrósio, Threlfall based, piecewise linear, and Bengisu and Akay. These friction force models have been briefly described earlier in Section 3. The response of the four bar linkage in terms of the kinematics of the rocker links is plotted in the diagrams of Fig. 8 for the different friction force models. From these plots, it can be observed that the general response of the mechanism is quite similar, as it can be seen the Figs. 8a-c. In fact, the main differences among the friction models can occur in the vicinity of null relative sliding velocity. In order to observe the possible discrepancies in terms of system's response, a detailed view is displayed in Fig. 8d for the rocker z-acceleration, in which the relative sliding velocity is close to zero. The models where the static friction is taken into account exhibit smaller peaks in the acceleration curve, in particular the Ambrósio and Threlfall models, as it is visible in Fig. 8d. Since the friction force models have small differences on the system's response, in what follows, the Threlfall based friction model is the only one considered for further analysis.


(a)

(b)

(c)

(d)

(e)

(f)

7
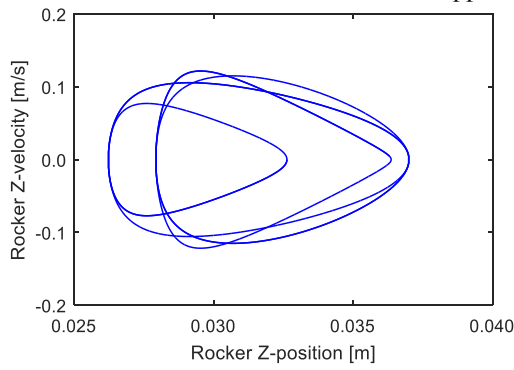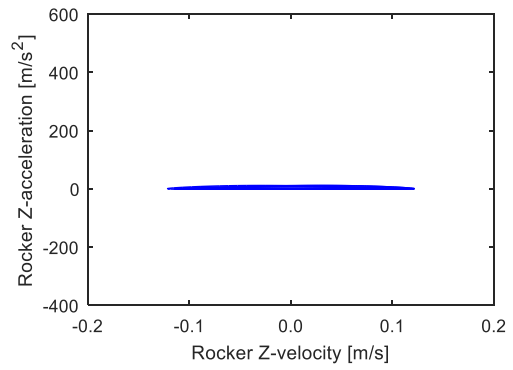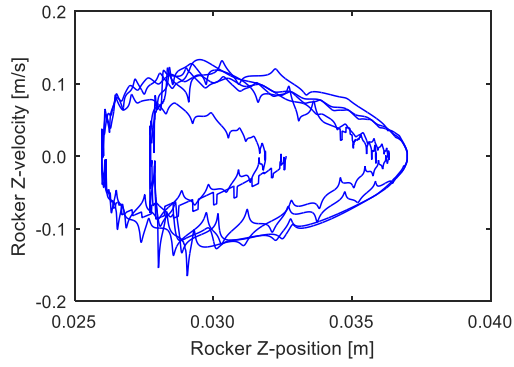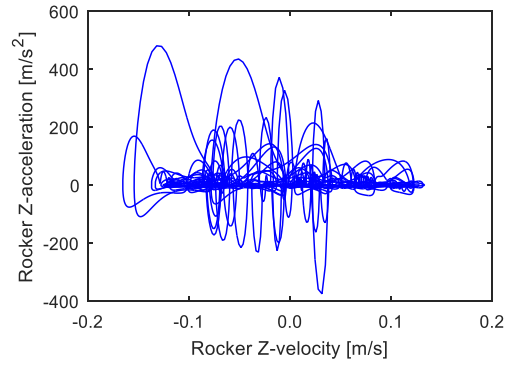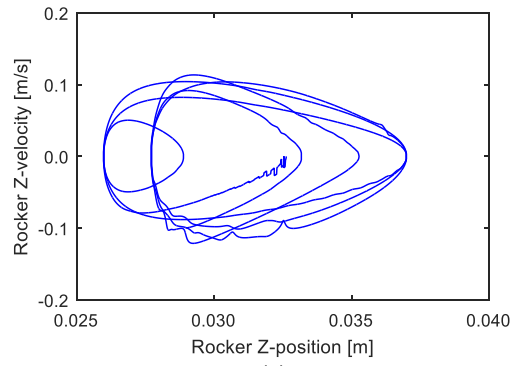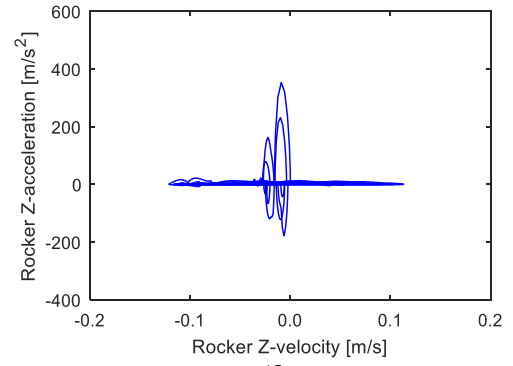
Figure 7: Portrait phases of rocker *Z*-position versus *Z*-velocity and rocker *Z*-velocity versus *Z*-acceleration: (a)-(b) ideal joint; (c)-(d) frictionless clearance joint, and (e)-(f) clearance joint with friction

The influence of the radial clearance size at the spherical joint clearance is also analyzed for the case modeled with the Threlfall friction approach. For this purpose, four different clearance sizes are considered, namely 0.05, 0.1, 0.2 and 0.4 mm. Figure 9 shows rocker kinematics and mechanical energy variation for these four situations. As it was expected, the mechanism tends to present a similar response to the ideal case when the clearance size is very small. In fact, the behavior of the system tends to be less chaotic for smaller clearances. It can also be observed that the decrease of clearance leads to a more conservative system, as it can be observed in Fig. 9d relative to the variation of the mechanical energy of the mechanism.

Figure 10 shows the influence of the coefficient of friction on the response of the mechanism. Again the Threlfall based friction approach has been utilized and four different values for the kinetic coefficient of friction are considered, namely, 0.05, 0.1, 0.2 and 0.4. From the plots presented in Fig. 10, it can be observed that the higher the coefficient of friction is, the more energy is dissipated.

Finally, the computational efficiency for the different formulations of the spherical joint is examined here. In addition, the influence of the friction force model, the clearance size and fiction coefficient on the computational efficiency are studied. For this purpose, the number of functions evaluated during the numerical solution of the equations of motion is considered. Figure 11a shows that the introduction of a spherical joint with clearance penalizes the system's efficiency when compared with the ideal case. It is worth nothing though that the existence of friction at the clearance joint increases the computational efficiency, as it can be observed in the plots of Fig. 11a. In general, the friction force model utilized and the value of the clearance size do not significantly differ in terms of computational efficiency, as shown in Figs. 11b-c. However, for lower values of the friction coefficients, the simulations tend to be slower, as it is quite visible in the diagrams plotted in Fig. 11d.
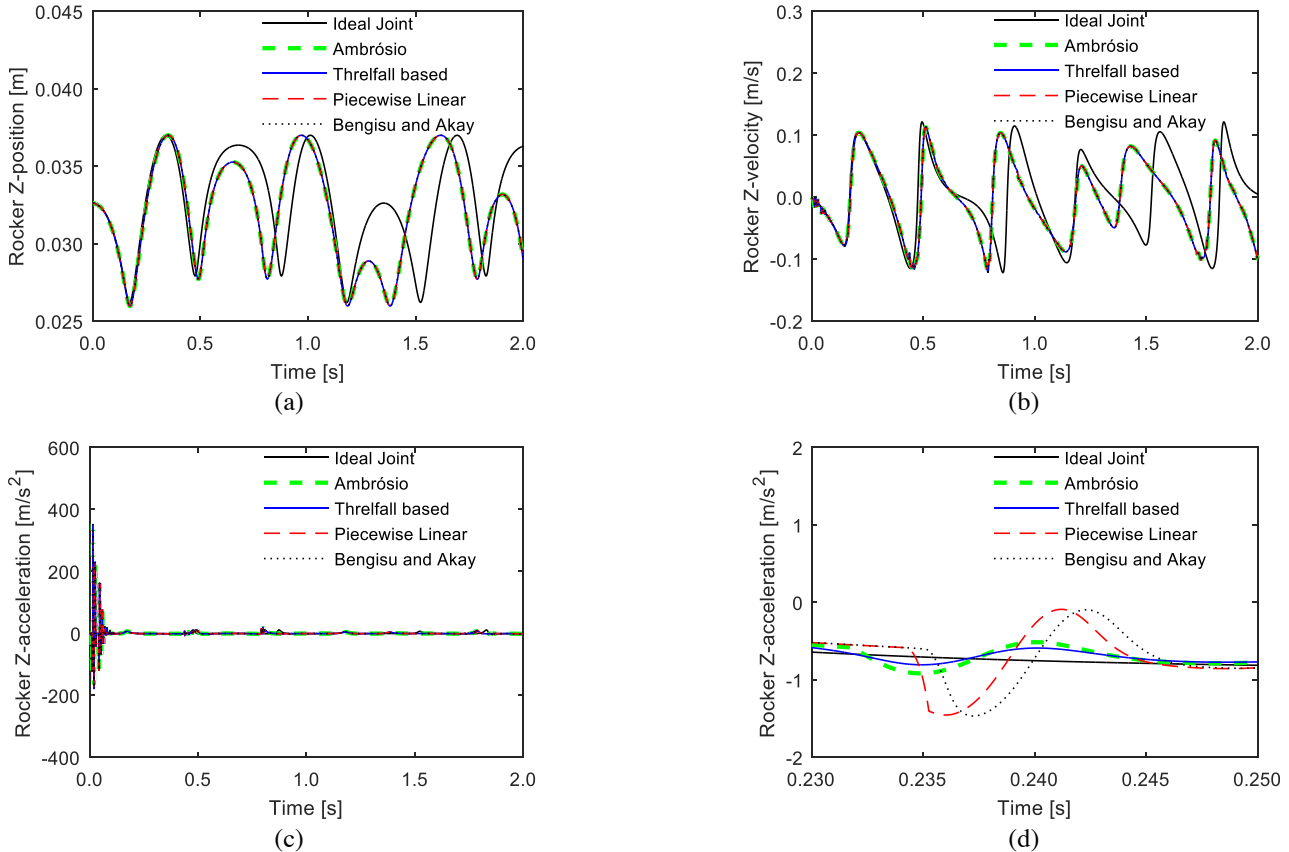

Figure 8: Influence of the friction force model on the four bar mechanism's response

(a)

(b)

(c)

(d)
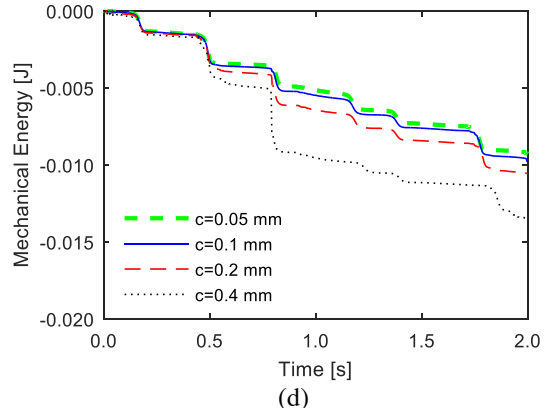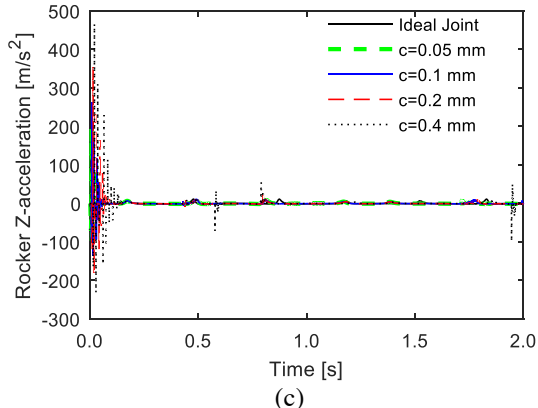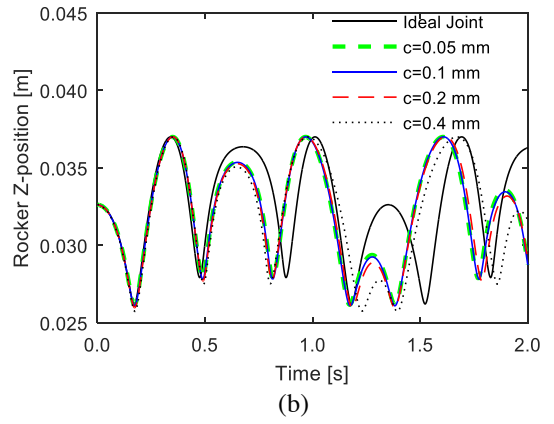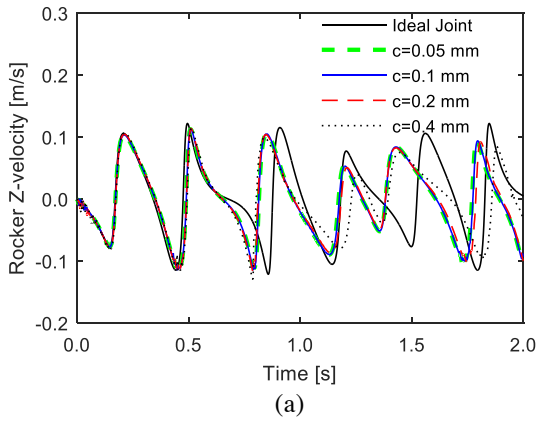
Figure 9: Influence of the clearance size on the four bar mechanism's response


(a)

(b)

(c)

(d)
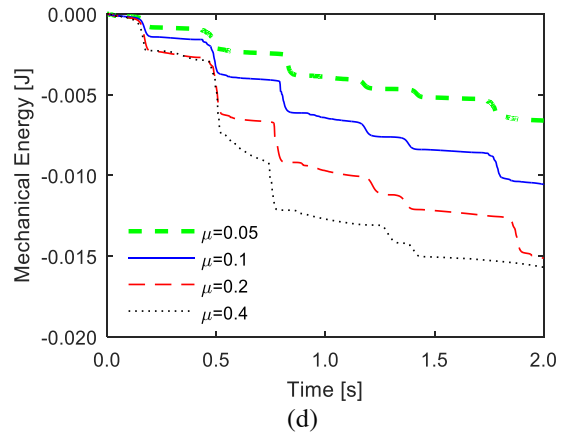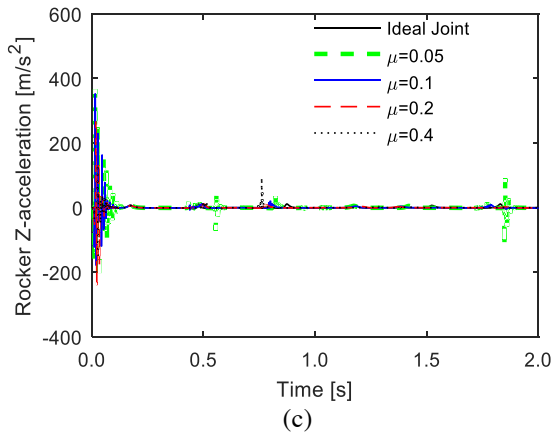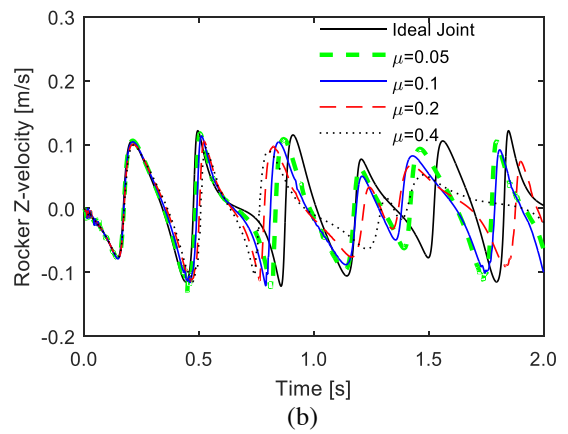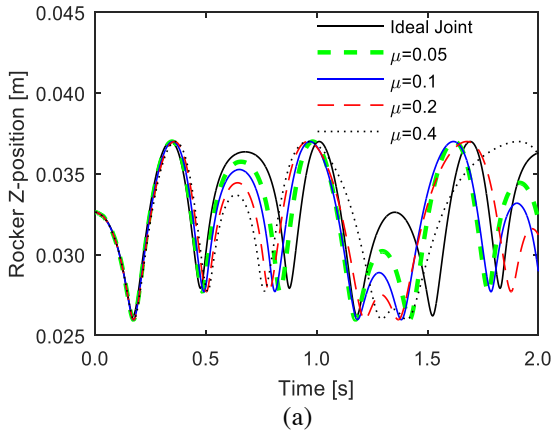
Figure 10: Influence of the coefficient of friction on the four bar mechanism's response
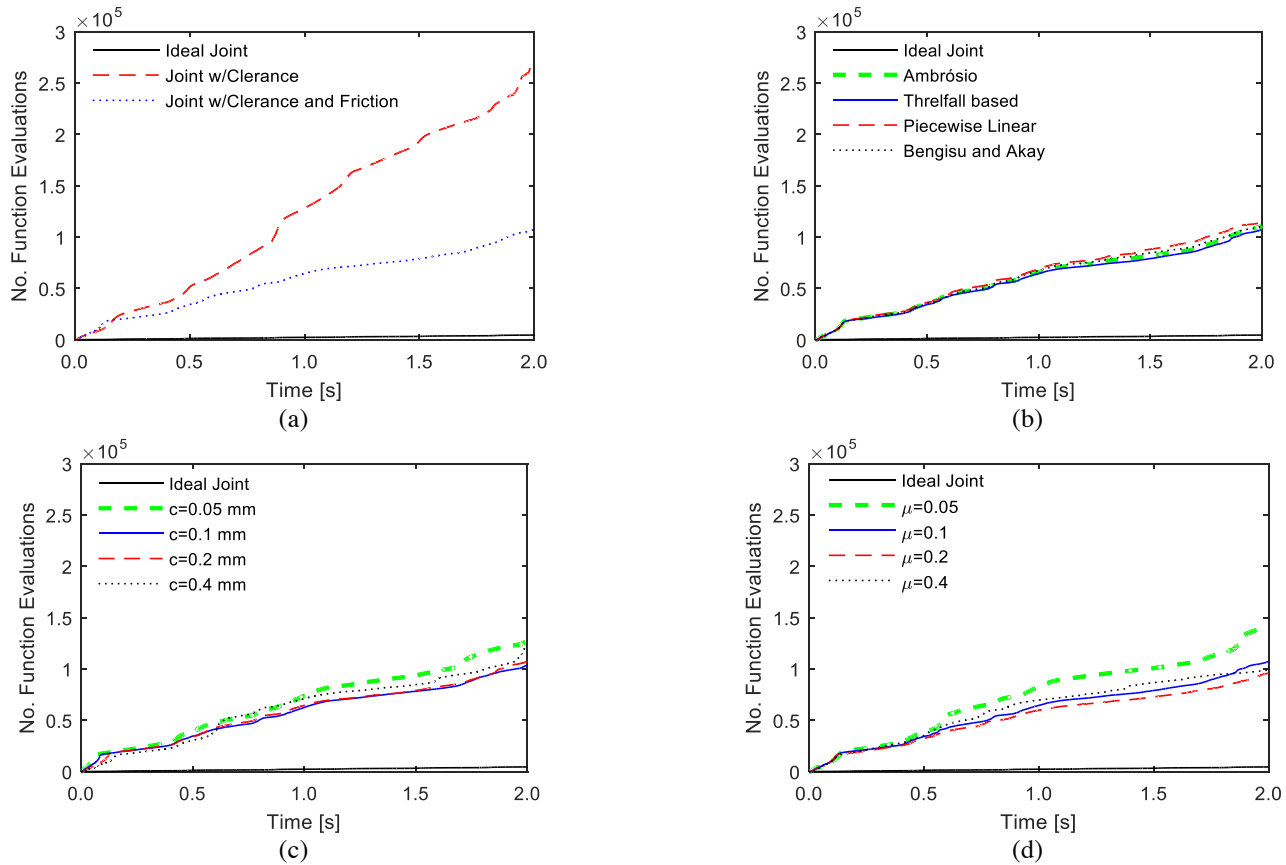
Figure 11: Effect of the joint model, friction force model, clearance size and friction coefficient on the computational efficiency

5. CONCLUDING REMARKS

The dynamic modeling and analysis of spatial mechanism with spherical clearance joint in the presence of friction has been presented in this work. In the sequel of this process, the main kinematic and dynamic aspects related to the modeling of spherical joints with clearance were first described under the framework of multibody systems methodologies. In a simple manner, the intra-joint contact-impact and friction forces developed at the spherical clearance joints are modeled using continuous contact force approaches, which account for the geometric, kinematic and material properties of the contact points. In particular, a dissipative normal contact force model as well as several different friction models are examined.

A classic spatial four bar mechanism with a spherical clearance joint was considered as a demonstrative application example to study the effect of joint modeling approaches. In addition, the effects of friction force model, friction coefficient value, and size of the clearance are investigated. In general, the presence of a clearance joint strongly affects the performance of the system, visible in terms of larger and abrupt peaks in the velocities and accelerations plots. It was also shown that the clearance size influences the behavior of the four bar mechanism, and the increase amplifies the resulting velocity and acceleration. In contrast, the presence of friction tends to stabilize the system's response and makes it less chaotic. The friction force model utilized however does not significantly affect the dynamic response of the mechanism. The value of the friction coefficient can influence the system's behavior, in terms of the dynamic response, as more mechanical energy is dissipated for larger friction coefficients. Finally, the computational efficiency from the different joint modeling approaches and scenarios analyzed in this work was also investigated.

REFERENCES

[1]   Goodman, T.P., 1962. Dynamic Effects of Backlash. Transaction of the 7th Mechanisms Conference, Purdue University, 128-138.
[2]   Garrett, R.E., Hall, A.S., 1969. Effect of Tolerance and Clearance in Linkage Design. Journal of Engineering for Industry, 91, 198-202.
[3]   Dubowsky, S., 1974. On Predicting the Dynamic Effects of Clearances in One-Dimensional Closed Loop Systems. Journal of Engineering for Industry, 96, 324-329.
[4]   Stoenescu, E.D., Marghitu, A.B., 2003. Dynamic analysis of a planar rigid-link mechanism with rotating slider joint and clearance. Journal of Sound and Vibration, 266(2), 394-404.
[5]   Parenti-Castelli, V., Venanzi, S., 2005. Clearance influence analysis on mechanisms. Mechanism and Machine Theory, 40(12), 1316-1329.
[6]   Flores, P., Lankarani, H.M., 2012. Dynamic Response of Multibody Systems with Multiple Clearance Joints. Journal of Computational and Nonlinear Dynamics, 7, 031003-13.
[7]   Zhang, Z., Xu, L., Flores, P., Lankarani, H.M., 2014. A Kriging Model for Dynamics of Mechanical Systems With Revolute Joint Clearances.

Journal of Computational and Nonlinear Dynamics, 9(3), 031013-031013-13.

[8] Chen, Y., Sun, Y., Chen, C., 2016. Dynamic analysis of a planar slider-crank mechanism with clearance for a high speed and heavy load press system. Mechanism and Machine Theory, 98, 81-100.

[9] Li, Y., Chen, G., Sun, D., Gao, Y., Wang, K., 2016. Dynamic analysis and optimization design of a planar slider–crank mechanism with flexible components and two clearance joints. Mechanism and Machine Theory, 99, 37-57.

[10] Daniel, G.B., Machado, T.H. Cavalca, K.L., 2016. Investigation on the influence of the cavitation boundaries on the dynamic behavior of planar mechanical systems with hydrodynamic bearings. Mechanism and Machine Theory, 99, 19-36.

[11] Wilson, R., Fawcett, J.N., 1974. Dynamics of the Slider-Crank Mechanism with Clearance in the Sliding Bearing. Mechanism and Machine Theory, 9, 61-80.

[12] Farahanchi, F., Shaw, S., 1994. Chaotic and Periodic Dynamics of a Slider-Crank Mechanism with Slider Clearance. Journal of Sound and Vibration, 177(3), 307-324.

[13] Thümmel, T., Funk, K., 1999. Multibody Modeling of Linkage Mechanisms including Friction, Clearance and Impact. Proceedings of 10th World Congress on TMM in Oulu, Finland, Oulu University Press, Vol. 4, 1375-1386.

[14] Flores, P., Ambrósio, J., Claro, J.C.P., Lankarani, H.M., 2008. Translational joints with clearance in rigid multibody systems. Journal of Computational and Nonlinear Dynamics, 3(1), 0110071-10.

[15] Flores, P., Leine, R., Glocker, C., 2010. Modeling and analysis of planar rigid multibody systems with translational clearance joints based on the non-smooth dynamics approach. Multibody System Dynamics, 23(2), 165-190.

[16] Zhang, J., Wang, Q., 2016. Modeling and simulation of a frictional translational joint with a flexible slider and clearance. Multibody System Dynamics, 38(4), 367-389.

[17] Flores, P., Ambrósio, J., Claro, J.C.P., Lankarani, H.M., 2006. Spatial revolute joints with clearance for dynamic analysis of multibody systems. Proceedings of the Institution of Mechanical Engineers, Part-K Journal of Multi-body Dynamics, 220(4), 257-271.

[18] Tian, Q., Sun, Y., Liu, C., Hu, H., Flores, P., 2013. Elastohydrodynamic lubricated cylindrical joints for rigid-flexible multibody dynamics. Computers and Structures, 114-115, 106-120.

[19] Tian, Q., Xiao, Q., Sun, Y., Hu, H., Flores, P., 2015. Coupling dynamics of a geared multibody system supported by Elastohydrodynamic lubricated cylindrical joints. Multibody System Dynamics, 33, 259-284.

[20] Haines, R.S., 1985. An Experimental Investigation into the Dynamic Behaviour of Revolute Joints with Varying Degrees of Clearance. Mechanism and Machine Theory, 20, 221-231.

[21] Stein, J.L., Wang, C-H., 1996. Automatic detection of clearance in mechanical systems: Experimental validation. Mechanical Systems and Signal Processing, 10(4), 395-409.

[22] Erkaya, S., Uzmay, I., 2010. Experimental investigation of joint clearance effects on the dynamics of a slider-crank mechanism. Multibody System Dynamics, 24 (1), 81-102.

[23] Koshy, C.S., Flores, P., Lankarani, H.M., 2013. Study of the effect of contact force model on the dynamic response of mechanical systems with dry clearance joints: computational and experimental approaches. Nonlinear Dynamics, 73(1-2), 325-338

[24] Erkaya, S., Doğan, S., Ulus, S., 2015. Effects of joint clearance on the dynamics of a partly compliant mechanism: Numerical and experimental studies. Mechanism and Machine Theory, 88, 125-140.

[25] Crowthera, A.R., Singha, R., Zhangb, N., Chapman, C., 2007. Impulsive response of an automatic transmission system with multiple clearances: Formulation, simulation and experiment. Journal of Sound and Vibration, 306, 444-466.

[26] Ambrósio, J., Verissimo, P., 2009. Improved bushing models for general multibody systems and vehicle dynamics. Multibody System Dynamics, 22(4), 341-365.

[27] Wang, G., Liu, H., Deng, P., Yin, K., Zhang, G., 2016. Dynamics Analysis of 4-SPS/CU Parallel Mechanism considering 3-D Wear of Spherical Joint with Clearance. Journal of Tribology, DOI:10.1115/1.4034763

[28] Jing, Z., Hong-Wei, G., Rong-Qiang, L., Zong-Quan, D., 2015. Nonlinear Characteristic of Spherical Joints with Clearance. Journal of Aerospace and Technology Management, 7(2), 179-184.

[29] Quental, C., Folgado, J., Ambrósio, J., Monteiro, J., 2013. Multibody system of the upper limb including a reverse shoulder prosthesis. Journal of Biomechanical Engineering, 135(11), 111005.

[30] Askari, E., Flores, P., Dabirrahmani, D., Appleyard, R., 2014. Nonlinear vibration and dynamics of ceramic on ceramic artificial hip joints: a spatial multibody modeling. Nonlinear Dynamics, 76, 1365-1377.

[31] Askari, E., Flores, P., Dabirrahmani, D., Appleyard, R., 2015. Dynamic modeling and analysis of wear in spatial hard-on-hard couple hip replacements using multibody systems methodologies. Nonlinear Dynamics, 82(1), 1039-1058.

[32] Bauchau, O.A., Rodriguez, J., 2002. Modeling of Joints with Clearance in Flexible Multibody Systems. International Journal of Solids and Structures, 39(1), 41-63.

[33] Orden, J.C.G., 2005. Analysis of Joint Clearances in Multibody Systems. Multibody System Dynamics, 13, 401-420.

[34] Liu, C-S., Zhang, K., Yang, L., 2006. Normal force-displacement relationship of spherical joints with clearances. Journal of Computational and Nonlinear Dynamics, 1(2), 160-167.

[35] Flores, P., Ambrósio, J., Claro, J.C.P., Lankarani, H.M., 2006. Dynamics of multibody systems with spherical clearance joints. Journal of Computational and Nonlinear Dynamics, 1(3), 240-247.

[36] Tian, Q., Zhang, Y., Chen, L., Flores, P., 2009. Dynamics of spatial flexible multibody systems with clearance and lubricated spherical joints. Computers and Structures, 87 (13-14), 913-929.

[37] Wang, G., Liu, H., Deng, P., 2015. Dynamics Analysis of Spatial Multibody System With Spherical Joint Wear. Journal of Tribology, 137(2), 021605.

[38] Wang, G., Liu, H., 2015. Dynamics Analysis of 4-SPS/CU Parallel Mechanism with Spherical Joint Clearance. Journal of Mechanical Engineering, 51(1), 43-51.

[39] Zheng, E., Zhu, R., Zhu, S., Lu, X., 2016. A study on dynamics of flexible multi-link mechanism including joints with clearance and lubrication for ultra-precision presses. Nonlinear Dynamics, 83(1), 137-159.

[40] Nikravesh, P.E., 1988. Computer Aided Analysis of Mechanical Systems. Prentice Hall, Englewood Cliffs, New Jersey.

[41] Hertz, H., 1896. On the contact of solids - On the contact of rigid elastic solids and on hardness. (Translated by D.E. Jones and G.A. Schott), Miscellaneous Papers, Macmillan and Co. Ltd., London, England, 146-183.

[42] Goldsmith, W., 1960. Impact – The theory and physical behaviour of colliding solids. Edward Arnold Ltd, London, England.

[43] Lankarani, H.M., Nikravesh, P.E., 1990. A Contact Force Model With Hysteresis Damping for Impact Analysis of Multibody Systems. Journal of Mechanical Design, 112, 369-376.

[44] Alves, J., Peixinho, N., Silva, M.T., Flores, P., Lankarani, H., 2015. A comparative study on the viscoelastic constitutive laws for frictionless contact interfaces in multibody dynamics. Mechanism and Machine Theory, 85, 172-188.

[45] Olsson, H., Åström, K.J., Canudas de Wit, C., Gäfvert, M., Lischinsky, P., 1998. Friction Models and Friction Compensation. European Journal of Control, 4(3), 176-195.

[46] Berger, E.J., 2002. Friction modeling for dynamic system simulation. Applied Mechanics Reviews, 55(6), 535-577.

[47] Marques, F., Flores, P., Claro, J.C.P., Lankarani, H.M., 2016. A survey and comparison of several friction force models for dynamic analysis of multibody mechanical systems. Nonlinear Dynamics, 86(3), 1407-1443.

[48] Coulomb, C.A., 1785. Théorie des machines simples, en ayant égard au frottement de leurs parties, et à la roideur des cordages. Mémoire de Mathématique et de Physique, Paris, France.

[49] Threlfall, D.C., 1978. The inclusion of Coulomb friction in mechanisms programs with particular reference to DRAM au programme DRAM. Mechanism and Machine Theory, 13(4), 475-483.

[50] Rooney, G.T., Deravi, P., 1982. Coulomb Friction in Mechanism Sliding Joints. Mechanism and Machine Theory, 17, 207-211.

[51] Ambrósio, J.A.C., 2003. Impact of Rigid and Flexible Multibody Systems: Deformation Description and Contact Model. Virtual Nonlinear Multibody Systems, 103, 57-81.

[52] Stribeck, R., 1902. Die wesentlichen Eigenschaften der Gleitund Rollenlager. Zeitschrift des Vereines Deutscher Ingenieure, 46(38), 1342-1348, 1432-1438; 46(39), 1463-1470.

[53] Bo, L.C., Pavelescu, D., 1982. The friction-speed relation and its influence on the critical velocity of stick-slip motion. Wear, 82(3), 277-289.

11

[54] Bengisu M.T., Akay, A., 1994. Stability of Friction-Induced Vibrations in Multi-Degree-of-Freedom Systems. Journal of Sound and Vibration, 171(4), 557-570.

[55] Baumgarte, J., 1972. Stabilization of constraints and integrals of motion in dynamical systems. Computer Methods in Applied Mechanics and Engineering, 1, 1-16.

[56] Flores, P., Machado, M., Seabra, E., Silva, M.T., 2011. A parametric study on the Baumgarte stabilization method for forward dynamics of constrained multibody systems. ASME Journal of Computational and Nonlinear Dynamics, 6(1), 011019 (9p).